BASIC SCIENCE

Nanomedicine: Nanotechnology, Biology, and Medicine
13 (2017) 2555–2564

Original Article

nanomedjournal.com

Rationally designed peptide nanosponges for cell-based cancer therapy

Hongwang Wang, PhD[a,1], Asanka S. Yapa, PhD[a,1], Nilusha L. Kariyawasam, BSc[a,1], Tej B. Shrestha, PhD[b,1], Madumali Kalubowilage, PhD[a], Sebastian O. Wendel, PhD[a,b], Jing Yu, MS[a], Marla Pyle, MSc[a], Matthew T. Basel, PhD[b], Aruni P. Malalasekera, PhD[a], Yubisela Toledo, BSc[a], Raquel Ortega, BSc[a], Prem S. Thapa, PhD[c], Hongzhou Huang, PhD[d], Susan X. Sun, PhD[d], Paul E. Smith, PhD[a], Deryl L. Troyer, PhD, DVM[b], Stefan H. Bossmann, PhD[a,*]

[a]*Department of Chemistry, Kansas State University, Manhattan, KS, USA*
[b]*Department of Anatomy & Physiology, Kansas State University, Manhattan, KS, USA*
[c]*Microscopy and Analytical Imaging Laboratory, University of Kansas, Lawrence, KS, USA*
[d]*Grain Science and Industry, Kansas State University, Manhattan, KS, USA*

Received 15 March 2017; accepted 12 July 2017

Abstract

A novel type of supramolecular aggregate, named a "nanosponge" was synthesized through the interaction of novel supramolecular building blocks with trigonal geometry. The cholesterol-$(K/D)_n$DEVDGC)$_3$-trimaleimide unit consists of a trigonal maleimide linker to which homopeptides (either K or D) of variable lengths (n = 5, 10, 15, 20) and a consensus sequence for executioner caspases (DEVDGC) are added via Michael addition. Upon mixing in aqueous buffer cholesterol-$(K)_n$DEVDGC)$_3$-trimaleimides and a 1:1 mixture of cholesterol-$(K/D)_n$DEVDGC)$_3$-trimaleimides form stable nanosponges, whereas cholesterol-$(D)_n$DEVDGC)$_3$-trimaleimide is unable to form supramolecular aggregates with itself. The structure of the novel nanosponges was investigated through explicit solvent and then coarse-grained molecular dynamics (MD) simulations. The nanosponges are between 80 nm and several micrometers in diameters and virtually non-toxic to monocyte/macrophage-like cells.

Key words: Nanosponges; Drug delivery; Nanomaterials; Supramolecular; Aggregation; Explicit solvent molecular dynamics simulations; Coarse-grained molecular dynamics simulations

Classic liposomes and peptide vesicles

Targeted delivery of therapeutics to the tumor site is of vital importance in cancer treatment. This approach is able not only to maximize the treatment efficacy of therapeutics at the cancer site(s), but also to minimize the side effects caused by the therapeutics in conventional cancer treatment.[1,2] One method to achieve targeting delivery is to use a delivery modality designed to carry the therapeutics to the desired site, and then release them in the tumor.[3–6] Liposomes are a well-recognized example of drug delivery devices. Composed of a simple lipid bilayer, liposomes are non-cytotoxic, biocompatible, biodegradable, and capable of integrating or encapsulating large payloads of both hydrophilic and hydrophobic drugs.[7] Drugs incorporated into these nanocarriers can be accumulated in tumor tissue through the enhanced permeability and retention (EPR) effect.[8–10] Numerous liposome based drugs have been approved by the FDA, and many more are at different stages of clinical trials.[11] Despite their successes, liposomes have limitations. It is noteworthy that the preparation of liposome based drug requires

Abbreviations: PBS, phosphate-buffered saline buffer; AFM, Atomic Force Microscopy; TEM, Transmission Electron Microscopy; HBTU, (2-(1H-benzotriazol-1-yl)-1,1,3,3-tetramethyluronium hexafluorophosphate); DIEA, N,N-Diisopropylethylamine; CDI, (carbonyl-di-imidazole); TIPS, triisopropylsilane; HEPES, 4-(2-hydroxyethyl)-1-piperazineethanesulfonic acid.

This work was funded by NSF (DMR 1242765 and CBET EAGER 1656989), and the Johnson Cancer Center at Kansas State University.

The authors declare no competing financial interest.

* Corresponding author at: Kansas State University, Department of Chemistry, Manhattan, KS 66506-0401.

E-mail address: sbossman@ksu.edu (S.H. Bossmann).

[1] These authors have contributed equally.

http://dx.doi.org/10.1016/j.nano.2017.07.004
1549-9634/

multistep procedures (i.e., hydration,[12,13] sonication,[14,15] extrusion,[16,17] using a size selective column,[18] etc.) in order to obtain narrow particle size distribution and separation from unloaded drugs. These tedious processes are associated with a high risk of damaging the entrapped drugs. Furthermore, the EPR effect is only slightly selective, thus achieving rarely more than 5 percent delivery of a nanotherapeutic drug to the tumor site(s).[8–10] Finally, liposomes are prone to systemic leaking of drugs, especially at longer circulation times.[19]

Self-assembling peptides are an attractive alternative to liposomes. For example, short amphiphilic sequences, acetyl-AAVVLLLW-$(E)_{n=2/7}$-COOH, form nanosized vesicles spontaneously in aqueous media at neutral pH. Hydrophilic molecules can be incorporated inside the vesicles.[20] Longer block copolypeptides poly(L-lysine)-*b*-poly(L-leucine), K_xL_y (x = 20 to 80, y = 10 to 30), form stable vesicles and micelles in aqueous solution with size ranging from 1 to 10 μm in diameter. These assemblies showed high degrees of membrane fluidity; as a result, they can be resized with precise control from ten to hundreds nanometers in diameter using liposome-based extrusion techniques.[21] The Tomich group reported two branched peptides with different lengths, mimicking diacyl glycerols, form water-filled vesicles, which can entrap water soluble dyes.[22–25]

The EPR effect works well in mice, but not in humans

During the last decade, it has become more and more evident that both, classic liposomes and peptide vesicles are facing the problem of ineffective drug delivery in humans. It is an emerging paradigm that the Enhanced Permeation and Retention Effect (EPR) works well in mouse models of cancer, but not in the clinic.[10,26,27] Drug transport as a payload of either stem cells[28] or defensive cells,[27] which migrate to tumors following their cytokine/chemokine secretion, is a new concept that has been proven effective in animal models. Currently, clinical translation of cell-based treatment methods for cancer and other diseases is rapidly progressing.[29] Therefore, we have developed "peptide nanosponges" for efficient targeting of defensive cells in peripheral blood, as well as cultured stem cells.

Peptide nanosponges

Peptide nanosponges that are reported here, are capable of effectively delivering their payload to defensive cells and stem cells. Especially autologous cells have the potential of truly personalized medicine when treating solid tumors and metastases.[30]

Here, we report the synthesis of a series of $(K)_n$DEVDGC, and $(D)_n$DEVDGC peptide sequences, where *n* equals to 5, 10, 15, 20 respectively. We have capped the N-terminal of the peptides with cholesterol, and further linked the peptides to a trimaleimide scaffold via Michael-addition.[31] We have obtained one positively and one negatively charged adduct [$(\text{cholesterol-}(K)_n\text{DEVDGC})_3$-trimaleimide and $(\text{cholesterol}(D)_n\text{DEVDGC})_3$-trimaleimide]. Upon mixing of the adduct pairs (*n* equals to 15 or 20) equimolarly under physiological conditions, nanosponges of very low polydispersity form instantaneously, which were characterized with dynamic light scattering (DLS), transmission electron microscopy (TEM), and atomic force microscopy (AFM).

Our computer modeling has indicated that the structure of the nanosponges is indeed "sponge-like": numerous hydrophilic and hydrophobic nanodomains exist in direct proximity. We attribute the novel (bio)physical properties of the nanosponges to their formerly unknown structure (Figure 1).

Our studies demonstrated that hydrophobic molecules, for example the cyanine 3.0 dye PKH26, can be incorporated inside these nanosponges. In the presence of cancer related proteases (e.g. caspase-3, 6 or 7[32]), these nanovesicles can be – principally – digested, leading to the possibility of triggered release of the payload. We found that the nanosponges are essentially non-toxic, and that these cells internalize them with high efficiency.

Based on these proof-of-concept experiments, our novel peptide-based nanosponges are very well suited for applications in specific drug delivery to solid tumors and metastases by means of cell-based therapy.

Methods

Trimaleinimide scaffold synthesis

A flexible trimaleinimide scaffold was synthesized by means of a two-step reaction. In the first step, reacting tris(2-aminoethyl) amine with 3 equivalents of maleic anhydride in acetic acid at room temperature produces the trimaleimic acid adduct.[33] In the second step, the trimaleimic acid adduct and sodium acetate were heated in acetic anhydride for 30 min at 100 °C to give the desired product.[34] The crude product was recrystallized from saturated ethyl acetate, and fully characterized by ^1H, ^{13}C NMR, and single crystal x-ray analysis (see SI section).

Peptide synthesis

Oligopeptides were synthesized by means of solid phase peptide synthesis on 2-chlorotrityl resin.[35,36] Three equivalents of F_{moc} (N-(9-fluorenyl)methoxycarbonyl) protected amino acid and HBTU were dissolved in a DIEA/DMF solution, and added to the 2-chlorotrityl resin preloaded with 0.20 mmol of amino acid per g. The solution was drained from the resin after 30 min of reaction. This process was repeated one more time. Then, the F_{moc} group of the newly introduced amino acid was removed by using 20% (v/v) piperidine in DMF. Following this procedure, stepwise addition of F_{moc}-protected amino acids resulted in the desired peptides. The N-terminal of the peptides was capped with cholesterol while still being on the resin by reacting with CDI activated cholesterol in DMF solution.[35,36] The final product was cleaved off the resin in TFA/water/TIPS (95:2.5:2.5, v/v/v) cocktail for 3 h at room temperature.[36] White solid product formed when adding the cocktail into cold anhydrous diethyl ether. The product was collected by centrifugation (3000 rpm, 10 min), washed with cold diethyl ether for three times, and dissolved in water prior to lyophilization. The products were purified by using a GE peptide column (mobile phase: aqueous 0.05 M TEA/acetic acid buffer, pH = 7.0), and dried in high vacuum.

Cholesterol-peptide-trimaleimide adduct formation

3.5 equivalents of cholesterol-peptide and 1 equivalent of trimaleimide were dissolved in deoxygenated PBS buffer (pH =

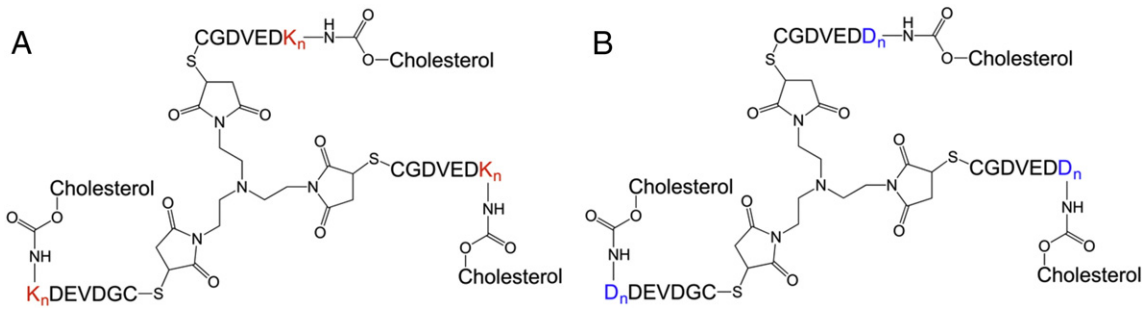

Figure 1. Tri-maleimide based peptide structures: components for the spontaneous formation of nanosponges. (**A**) Lysine-based materials, n = 5, 10, 15, 20. (**B**) Aspartic acid-based materials, n = 5, 10, 15, 20.

7.4), and stirred under argon atmosphere for 24 h.[37] After removing the solvent by lyophilization, the crude product was purified by dialysis (molecular weight cutoff 3500) against distilled water. The final product inside the membrane bag was lyophilized and further dried under high vacuum.

Nanosponge formation and DLS characterization

Separate solutions of (cholesterol-$(K)_n$DEVDGC)$_3$-trimaleimide and (cholesterol-$(D)_n$DEVDGC)$_3$-trimaleimide in deoxygenated PBS buffer were prepared and filtered through 200 μm filters. The prepared stock solutions were 0.050 mM and 0.50 mM. All other stock solutions were prepared by diluting the original solutions with deoxygenated PBS buffer. The two solutions were quickly mixed and vortexed for 30 s. The hydrodynamic diameters and polydispersity indexes (PDI) of the formed nanosponges were measured by dynamic light scattering (DLS, ZetaPALS, Brookhaven Instruments Corp., Holtsville, NY).[38] All measurements were carried out at 298 K, using 658 nm laser wavelength, and 90° detection angle. Data were collected from an average of three measurements over 60 s. DLS was also used to estimate the critical micellar concentration (cmc) of the nanosponges.

AFM characterization

Samples for atomic force microscopy (AFM) were prepared by adding one drop the nanosponge stock solution (0.050 M of each component in PBS) onto a freshly peeled MICA sheet, followed by removing of the solvent by using a gentle nitrogen stream (2 min). AFM images were taken by the Bruker Innova AFM image system (Bruker, Camarillo, CA) utilizing TESPA-HAR probes in tapping mode. The spring constant of the tip was 50 N/m and the frequency was 350 kHz. The set point, P gain and I gain were set at 1.2, 0.6 and 0.5, respectively. The images were gathered with 256 × 256 pixel resolution at a scan rate of 1 Hz. The images were then analyzed by the Nanoscope software (Bruker).

TEM characterization

Samples for transmission electron microscopy (TEM) were prepared by dropping 10 μL of 0.005% type DK20 solution in PBS directly on a glow discharged TEM grid. Uranyl acetate was used as a positive staining agent. In all cases electron microscopy was performed at an accelerating voltage of 200 kV. Nanosponge morphology on HOPG was examined by bright-field and dark-field transmission electron microscopy (TEM) using a FEI Technai G_2 transmission electron microscope at an electron acceleration voltage of 200 kV. Dark-field TEM did not reveal a characteristic diffraction pattern. High resolution images were captured using a standardized, normative electron dose and a constant defocus value from the carbon-coated surfaces. All TEM measurements were performed at the Microscopy and Analytical Imaging Laboratory of the University of Kansas.[39]

Molecular dynamics simulations

Classical molecular dynamics were performed using the gromacs software.[40] Simulations using the all atom (AA) Gromos force field (FF) were performed in the NpT ensemble at 300 K and 1 bar using the v-rescale and Berendsen temperature and pressure algorithms,[41,42] respectively. Electrostatic interactions were evaluated using the particle mesh Ewald approach,[43] while van der Waals interactions were truncated at 1.5 nm. The timestep was 2 fs and all solute bonds were constrained using Lincs,[44] while all solvent bonds (and angles) were constrained using Settle.[45] The coarse-grained (CG) simulations were also performed in the NpT ensemble at 310 K and 1 bar using the v-rescale and Parrinello-Rahman temperature and pressure algorithms,[41,46] respectively, as suggested by the MARTINI FF developers (http://www.cgmartini.nl/). Electrostatic and van der Waals interactions were evaluated using shifted potentials with a relative permittivity of 15.[47] The timestep was 25 fs and all solute bonds were constrained using Lincs. The CG simulations were checked to ensure that there was no freezing of water beads by calculating the diffusion constants of water periodically during the simulations. A variety of system sizes were simulated with the largest involving 108 (cholesterol-$(K)_{20}$DEVDGC)$_3$-trimaleimide and 108 (cholesterol-$(D)_{20}$DEVDGC)$_3$-trimaleimide molecules, 2376 sodium ions, and 776,763 water beads in a 45 nm cube box for 4 μs. Details of the FFs are provided in the Supporting Information.

Entrapment of PKH26 within peptide nanosponges

PKH26 solution was prepared by dissolving 10 μL of the PKH26 ethanolic dye solution (Sigma-Aldrich) to 1.0 mL of Diluent C in a polypropylene centrifuge tube, followed by addition of double-distilled water (pH = 6.90) to bring the total volume to 2.0 mL (final PKH26 concentration 5.0×10^{-6} M). Equal molar amounts of cholesterol-$(K)_{20}$DEVDGC)$_3$-trimaleimide and cholesterol-$(D)_{20}$DEVDGC)$_3$-trimaleimide (1.0 mM of each component) were added to the above dye solution. After brief sonication, the homogeneous solution was incubated at 37 °C for 6

h without light exposure. The free dye was removed by passing the entire sample through a Sephadex G-50 gel filtration column using double-distilled water as eluent. The collected fractions containing the nanosponges were lyophilized to dryness, and re-hydrated with PBS buffer (pH = 7.4). The DLS measurement showed that the hydrodynamic diameters of the nanovesicles were between 110 to 130 nm.

Cell experiments and MTT assays

The cytotoxicity of the PKH26 containing nanosponges was assessed by utilizing the MTT assay[48] on RAW264.7 monocyte/macrophage-like cells.[35] Cell experiments were carried out in RPMI 1640 medium with 10% FBS. The percentage of viable cells was determined after 24 and 48 h of incubation. Cells were seeded in a T-25 flask. After 24 h of incubation at 37 °C and 5% CO_2, cells were re-plated in a 96 well plate at 20000/cm^2 density and further incubated for 24 h at 37 °C, 5% CO_2, to obtain 80% confluency before the nanosponges were added.

A concentration series of the nanosponge composed of (cholesterol-$(K)_{20}$DEVDGC)$_3$-trimaleimide and (cholesterol-$(D)_{20}$-DEVDGC)$_3$-trimaleimide (0.0, 0.1, 0.2, 0.5, 1.0, 2.0, 5.0, 10, 20, 40, 60, 80, 100 μmol L^{-1} in total, molar ratio 1:1) was prepared by dissolving the nanosponge components in the same media that were used for culturing the cells. Cells were incubated for 24/48 h at 37 °C. Eight replicates were prepared for each concentration. A portion of 10 μL of MTT reagent (5 mg/ml in PBS) was added to each well, and the plates were incubated for another 4 h at 37 °C. Finally, 100 μL of 10% sodium dodecyl sulfate in 0.010 M HCl was added into each well and incubated for 24 h at 37 °C. Their absorbance was recorded by using a plate reader at 550 nm and 690 nm. PBS solution was used as control for all the experiments. The solution with of μmol L^{-1} of nanosponge served as control.

RAW264.7 cells were imaged by using a Zeiss, Axiovert 40 CFL microscope with darkfield, brightfield, phase contrast and epifluorescence illumination, a camera system and Jenoptik, a ProgRes C3 Cool camera and ProgRes Capture Pro 2.10.0.0 software.

Results

DLS characterization of the nanosponges

The effective diameters and the polydispersity index (PDI) values of the nanosponges obtained by dynamic light scattering measurements (DLS) are summarized in Table 1. These results indicate that nanosponge formation depends on the number of lysine/aspartic acid units. Larger aggregates with higher polydispersity are observed when *n* equals 5. A significant decrease in both size and PDI (polydispersity index) was observed when increasing n to 10 (440 nm and 0.26). A further increase of K and D to 15 and 20 led to virtually mono-dispersed nanosponges with effective diameters of approx. 200 nm. It is noteworthy that the formation of these nanosponges is spontaneous upon mixing of the adduct solutions. Continuous monitoring by DLS for 12 h at 298 K revealed that the nanosponges are very stable in aqueous solution (PBS). For drug delivery purposes, we are particularly interested in nanosponges of 100 to 200 nm in diameter. Further characterization was carried out for n = 15 and 20. The corresponding correlation curves and number-averaged size distributions are shown in the SI section.

Table 1
Effective hydrodynamic diameters, polydispersity indexes (PDI), and standard deviations (SD) for (cholesterol-$(K)_n$DEVDGC)$_3$-trimaleimide + (cholesterol-$(D)_n$DEVDGC)$_3$-trimaleimide nanosponges (0.050 mM of each component in PBS).

n (D and K) =	Effective diameter ± SD (nm)	PDI ± SD
5	1200 ± 240	0.642 ± 0.07
10	440 ± 50	0.26 ± 0.04
15	200 ± 5.0	0.077 ± 0.01
20	180 ± 25	0.201 ± 0.03

Hydrodynamic diameters remained virtually constant for 12 h.

CMC of the nanosponges

In analogy to the formation of micelles, a critical concentration at which spontaneous aggregation to nanosponges occurs, was determined. This molar concentration was named cmc in analogy to "critical micellar concentration". In a monodisperse nanomaterial solution, the correlation curve (C(t)) of the measured data in a dynamic light scattering (DLS) experiment is a smooth, single exponential decay function. The diffusion coefficient (D) is proportional to the lifetime of the exponential decay and can be calculated by fitting the correlation curve to an exponential function. The hydrodynamic diameter of particles can be obtained by using a variation of the Stokes-Einstein equation with known D value.[49] Based on basic DLS theory, we measured the critical concentrations for the nanosponge formation of (cholesterol-$(K)_{20}$DEVDGC)$_3$-trimaleimide (K) and a 1:1 mixture of (cholesterol-$(D)_{20}$DEVDGC)$_3$-trimaleimide (D) and (cholesterol-$(K)_{20}$DEVDGC)$_3$-trimaleimide (K). The concentrations of D, K, and DK were stepwise increased by adding microliter aliquots from stock solutions of 0.50 M each to 1.0 mL of PBS buffer in a cuvette. The endpoint indication of this titration curve is the appearance of a smooth, single exponential decay correlation curve. (Cholesterol-$(D)_{20}$DEVDGC)$_3$-trimaleimide (D) did not show significant aggregation even after increasing its concentration to 0.30 mM. For (cholesterol-$(K)_{20}$DEVDGC)$_3$-trimaleimide a smooth, single exponential decay curve was observed when its concentration reached 0.080 mM. The equimolar mixture of (cholesterol)-$(D)_{20}$DEVDGC)$_3$-trimaleimide and (cholesterol-$(K)_{20}$DEVDGC)$_3$-trimaleimide (DK) showed most facile nanosponge formation at a concentration as low as 0.0050 mM (total concentration, 0.0025 mM (D) and 0.0025 mM (K)). In comparison, sodium dodecyl sulfate micelles possess a cmc of approx. 8 mM at 298 K, which corresponds to 2.31 g L^{-1}. In comparison, only about 0.055 g L^{-1} of type DK nanosponges and 0.90 g L^{-1} of type K nanosponges are required to achieve spontaneous aggregation (Figure 2).

AFM characterization

Figure 3 shows the AFM images of (cholesterol-$(D)_{15}$-DEVDGC)$_3$-trimaleimide/cholesterol-$(K)_{15}$DEVDGC)$_3$-trimaleimide and (cholesterol-$(D)_{20}$DEVDGC)$_3$-trimaleimide/ (cholesterol-$(K)_{20}$-DEVDGC)$_3$-trimaleimide nanosponges. Type DK15 nanosponges formed 0.5-0.9 μm aggregated bundles. The height of the bundles is

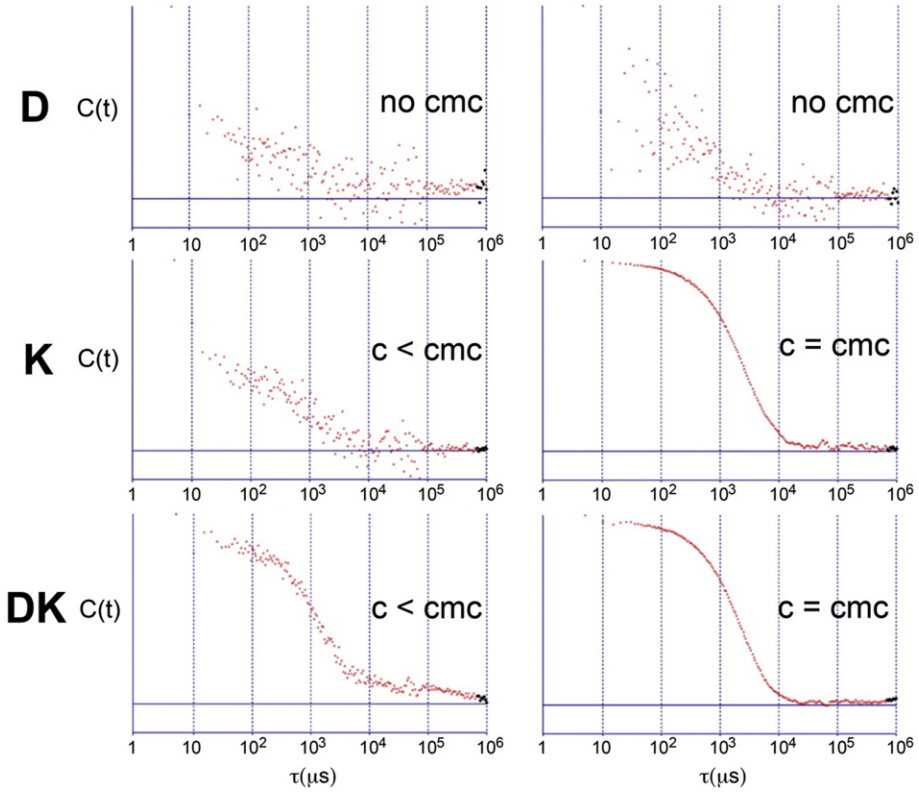

Figure 2. Correlation curves (C(t)) of dynamic light scattering measurements of (cholesterol-$(D)_{20}$DEVDGC)$_3$-trimaleimide (D), (cholesterol-$(K)_{20}$DEVDGC)$_3$-trimaleimide (K), and mixture (1/1 molar ratio) of both nanosponge components (DK) in 1× PBS buffer. In the left column, the concentrations of K, and DK are below the cmc (critical micellar concentration, here: concentration at which aggregation occurs). In the right column the concentrations are at their respective cmc (0.080 mM for type K and 0.0050 mM for type DK). No aggregation was observed for D in the concentration interval from 0.01 (left) to 0.30 mM (right).

between 150 to 250 nm. At higher magnification, it can be discerned that each bundle was formed by 3 to 5 smaller subunits. The diameter of the subunits ranges from 150 nm to 200 nm. Type DK20 nanosponges formed well defined individual nanosponges of 85 to 110 nm in size. Their height falls into the same range, indicating the formation of spherical nanosponges.

TEM characterization

TEM images for type DK20 nanosponges are shown in Figure 4. 2D projections of spherical sponges with diameters between 85 and 100 nm are clearly discernible (Figure 4, *A*). Their size distribution is displayed in Figure 4, *B*. However, smaller structures that are 35 to 45 nm in size can also be found in the TEM images. It is noteworthy that the exterior of the nanosponges acquired strong uranyl stains. This is an indication that cholesterol-$(D)_{20}$DEVDGC)$_3$-trimaleimide is enriched at the exterior of the nanostructures.

Molecular dynamics simulations

In an effort to elucidate the structure of the peptide aggregates we have performed all atom (AA) explicit solvent and coarse-grained (CG) molecular dynamics (MD) simulations. Technical aspects of the simulations, together with a detailed description of the models used, are provided in the Methods and the Supporting Information, respectively. However, before simulating the aggregation process itself it is important to check that the CG models are sufficiently accurate that reasonable results can be obtained. CG simulations are required as the systems under investigation involve large molecular aggregates. However, CG models generally provide rather crude representations of electrostatic interactions and conformational flexibility. As both these aspects are clearly present in the systems to be studied here, we have also investigated the ability of our CG models to mimic the more accurate AA explicit solvent analogues.

The simulation described here involves molecules for which no force fields (FFs) are currently available. Here, we describe our approach to provide reasonable descriptions of these systems using all atom (AA) and coarse-grained (CG) approaches. Highly accurate FFs for these systems would require significant development and may also necessitate experimental data that are not available. Hence, we have taken a more approximate, but practical, approach. We feel that this is appropriate as we are probing the overall behavior of the systems, and the requirement of CG models to study such large systems already introduces significant approximation.

The results from 100 ns AA and 1 μs CG MD simulations of the (cholesterol-$(K)_{20}$DEVDGC)$_3$-trimaleimide and (cholesterol-$(D)_{20}$-DEVDGC)$_3$-trimaleimide peptides have been compared. Electrostatic interactions followed the usual approach for the MARTINI models,[47] while partial conformational flexibility was introduced as

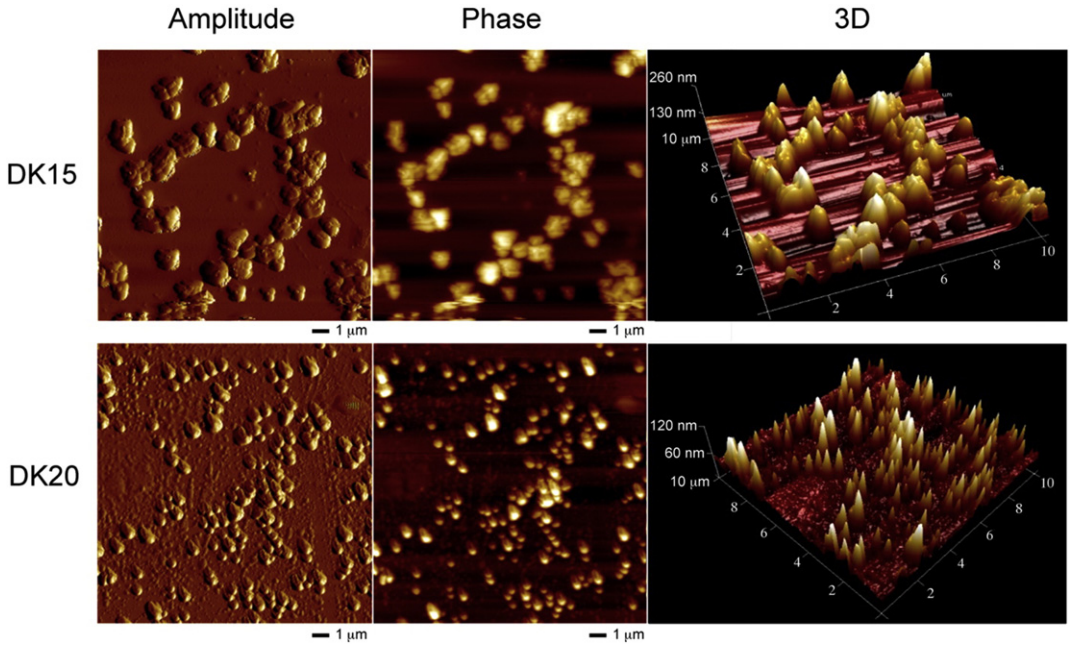

Figure 3. AFM (amplitude, phase, and 3D) images of type DK15 and type DK20 nanosponges. "15" and "20" refer to the number of D and K units in the oligopeptides that are attached to trimaleimide linkers.

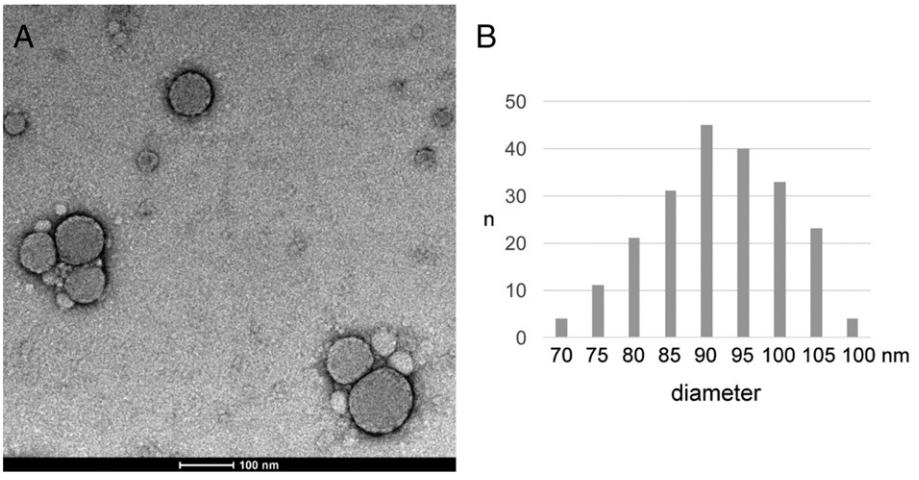

Figure 4. (**A**) TEM image of type DK20 nanosponges on graphite with uranyl acetate as positive staining. (**B**): Histogram of the size distribution of the larger nanosponges, obtained by using Image J (n: number of nanosponges counted in each group).[50]

described in the Supporting Information. The results are illustrated in Figure 5, *A*. The most notable behavior of the two peptide strands was the extended structures observed for (cholesterol-$(D)_{20}$-DEVDGC)$_3$-trimaleimide, and the collapsed structures observed for (cholesterol-$(K)_{20}$DEVDGC)$_3$-trimaleimide strands, as indicated by the AA simulations. The collapse of the (cholesterol-$(K)_{20}$-DEVDGC)$_3$-trimaleimide chain appears to require cholesterol as removal of this group eliminated any chain collapse (data not shown). This later observation is then in agreement with experimental data on poly-lys and poly-asp strands,[51–53] where the chains adopt extended or random coil structures. Clearly, the presence of cholesterol modifies this behavior. However, the same is not true for (cholesterol-$(D)_{20}$DEVDGC)$_3$-trimaleimide, which remains extended even in the presence of the cholesterol linkage. Most importantly, this difference in behavior is well reproduced in the CG simulations which also give rise to an extended (cholesterol-$(D)_{20}$DEVDGC)$_3$-trimaleimide and collapsed (cholesterol-$(K)_{20}$DEVDGC)$_3$-trimaleimide structures. Further examination of the (cholesterol-$(K)_{20}$DEVDGC)$_3$-trimaleimide simulation did not reveal any secondary structure formation upon collapse. Nevertheless, the identical behavior observed for the AA and CG models suggests that conformational

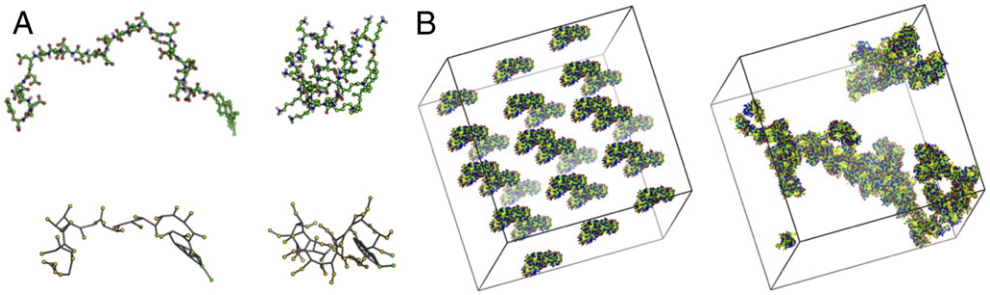

Figure 5. (**A**) Final structures obtained from the AA (top) and CG (bottom) simulations of (cholesterol-$(D)_{20}$DEVDGC)$_3$-trimaleimide (left) and (cholesterol-$(K)_{20}$DEVDGC)$_3$-trimaleimide (right). (**B**) Initial and final (4 μs) structures obtained from the CG simulation of (cholesterol-$(K)_{20}$DEVDGC)$_3$-trimaleimide and (cholesterol-$(D)_{20}$DEVDGC)$_3$-trimaleimide.

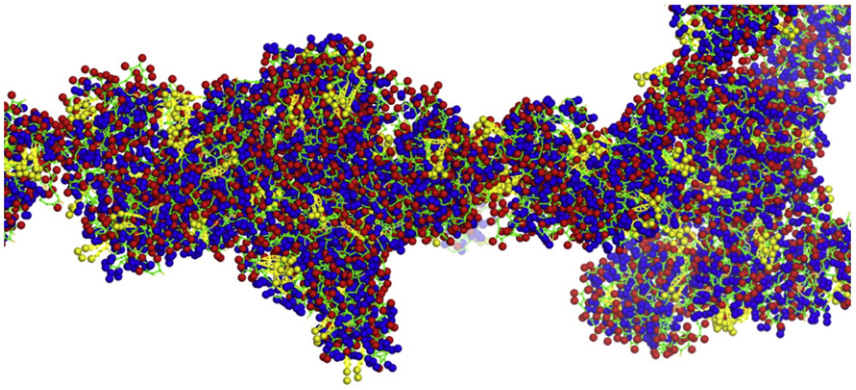

Figure 6. Expanded view of the final structure obtained from the CG MD simulations. The peptide backbone is displayed as green sticks, the Asp side chains are displayed as red balls, the Lys side chains are displayed as blue balls, while the cholesterol molecules are colored yellow. The structure resembles a "nanosponge" with hydrophobic and hydrophilic areas, as well as solvent-filled cavities.

flexibility and electrostatic interactions in these systems are sufficiently well represented that one can have confidence in the CG simulations.

The aggregation of equimolar mixtures of (cholesterol-$(K)_{20}$DEVDGC)$_3$-trimaleimide and (cholesterol-$(D)_{20}$DEVDGC)$_3$-trimaleimide was performed in two steps using just CG MD simulations. In the first step, we randomly placed four (cholesterol-$(K)_{20}$DEVDGC)$_3$-trimaleimides and four (cholesterol-$(D)_{20}$DEVDGC)$_3$-trimaleimides in a relatively small simulation box (15 nm in length), then transferred this peptide arrangement to a larger solvated box (40 nm in length) and simulated for 1 μs. This places the molecules in close proximity and they quickly formed a single relatively compact aggregate. In the second step the peptide aggregate was resolvated in a 15 nm length box, and then replicated in all three directions to form the final simulation box (45 nm in length) that was then simulated for 4 μs. During this period the smaller aggregates formed larger aggregates. This behavior is illustrated in Figure 6. Here, the smaller aggregates formed larger worm-like structures. Indeed, after 4 μs there were no isolated aggregates as all peptides chains contacted at least one other peptide chain. Clearly, the final structure obtained here does not represent that of a typical spherical vesicle, but more of a nanosponge. However, this is not too surprising as the peptides used here do not possess significant amphiphilic character compared to lipids, for example. Nevertheless, aggregation is observed in agreement with the experimental results described above, and other studies of poly-lys and poly-asp mixtures.[54]

While appearing largely amorphous the final structure obtained in Figure 5, *B* does display some interesting features. There was no strong evidence for secondary structure formation by either the (cholesterol-$(K)_{20}$DEVDGC)$_3$-trimaleimide or (cholesterol-$(D)_{20}$DEVDGC)$_3$-trimaleimide chains. While water did appear to be largely excluded from the chain contacts, there were visible cavities that appeared large enough to contain small molecules. An enlarged view of a section of the aggregate is display in Figure 6. Here one can see a preference of Asp side chains, over Lys side chains, for the surface. There was significant aggregation of cholesterol molecules to form stacked structures. However, these do not appear to be large enough to hold the aggregate together. Rather, electrostatic interactions appeared to be the main stabilizing force. The Asp-Lys side chain coordination numbers were determined to be 2.8 for the intermolecular contacts out to a distance of 0.7 nm.

Uptake of PKH26-containing nanosponges by RAW264.7 cells

Cell loading of the PKH26 entrapped nanosponges was tested on RAW264.7 monocyte/macrophage-like cells. This cell type

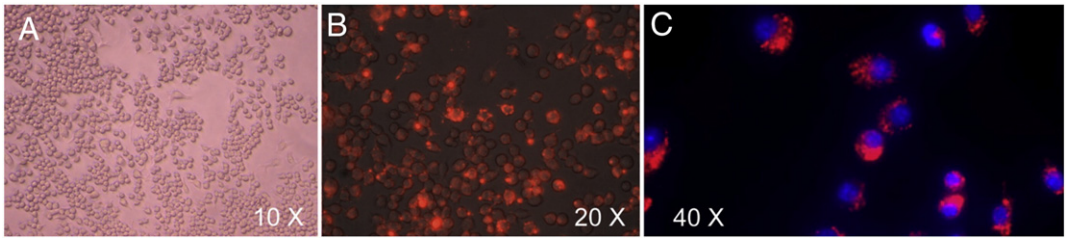

Figure 7. (**A**) RAW264.7 cells (control). (**B**) Fluorescent microscope image (taken with TRITC filter) of RAW264.7 cells after 2 h of incubation with 50 μM of PKH26-containing type DK nanosponges. (**C**) Fluorescence microscopy overlay of RAW264.7 cells featuring PKH26-containing nanosponges 72 h after uptake (image taken with TRITC filter) followed by a DAPI counterstain (image taken with UV filter).

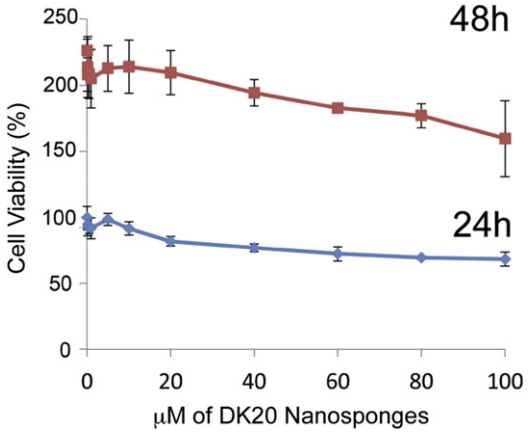

Figure 8. Cell viability of RAW264.7 cells as a function of type DK20 nanosponge concentration and incubation time (24 h and 48 h), as measured by the MTT assay.[35,55–57] Nanosponges were added to the cell culture medium in their respective concentrations (see experimental section).

was selected, because it can be used as carrier in cell-mediated cancer therapy.[55–57] Results indicated that type DK20 nanosponges can be loaded into RAW264.7 within 2 h. Under the fluorescence microscope, intensive red fluorescence spots can be discerned inside the cells, which are very different from labeling cells with free PKH26, which leads to uniform labeling (see SI). This indicates that after being taken up by these cells, the PKH26 is still entrapped inside the nanosponges. The PKH26-containing type DK20 nanosponges in Raw264.7 cells were studied over 24 h, 48 h, and 72 h. Virtually no leaching of the dye was observed by fluorescence microscopy within 72 h (Figure 7).

Cell toxicity of the peptide nanosponges

We have performed classic MTT cell proliferation assays[35,55–57] to measure the cell viability of RAW264.7 cells after incubation with PKH26-containing type DK20 nanosponges. As Figure 8 indicates, the type DK20 nanosponges are essentially not toxic to monocyte/macrophage-like cells, even at 100 μM concentration.

Discussion

A good targeted drug delivery system should have the following characteristics: a) composed by biocompatible and biodegradable materials, b) fast assembly and cargo loading, c) minimal systemic leaking during delivery, and d) fast release upon arrival at interested site.[58] We have designed (cholesterol-$(K)_n$ $DEVDGC)_3$-trimaleimide and (cholesterol-$(D)_n$$DEVDGC)_3$-trimaleimide units that both feature a trigonal linker, a cleavable sequence designed for executioner caspases-3,6, and 7 (DEVDGC[32]) and either an oligo-lysine or oligo-aspartic acid sequence of variable length (n = 5, 10, 15, 20). Whereas the cysteine at the C-terminus of each oligopeptide is used to attach it to the trigonal linker via Michael addition to maleimide,[31] the N-terminus is tethered to cholesterol, which has the function of a hydrophobic anchor. As Coarse-Grained Molecular Dynamics simulations indicate, a sponge-like dynamic structure is spontaneously assembled, due to the formation of ion pairs, intense hydrogen bonding, and the occurrence of hydrophobic regions and water-filled nanocavities. For nanosponges from (cholesterol-$(K)_{20}$$DEVDGC)_3$-trimaleimide/(cholesterol-$(D)_{20}$-$DEVDGC)_3$-trimaleimide units, AFM, TEM and DLS are in principal agreement about the diameter of the nanosponges. Furthermore, all three methods indicate the highly dynamic nature of the sponge-like aggregates, which is in very good agreement with the results obtained from Coarse-Grained Molecular Dynamics. The calculation discussed here predicts the relative enrichment of aspartate units at the nanosponges' surfaces. We can observe distinctly stronger staining at the exterior by uranyl acetate of the nanostructures observed in TEM. This is in perfect agreement with the predictions by modeling. The main difference between the TEM results and the principal outcome of the Molecular Dynamics Simulations is that the structures observed by TEM are spherical, whereas the simulated structures are not. The most probable cause for this discrepancy is that the TEM images were recorded on carbon-coated surfaces, which are very hydrophobic. Consequently, the cholesterol units are oriented towards the surface, causing a collapse of the 3D structure into a 2D coating. This effect is even more pronounced in high vacuum, which leads to a (partial) desiccation of the structure. Contrary to TEM, the structures observed by AFM resemble the results from Molecular Dynamics Simulations much closer.

The size of the nanosponges can be adjusted from several micrometers down to approx. 80 nm in diameter, depending on the concentration and the chemical composition (especially chain-length of the monopeptides (D or K)) of the supramolecular building blocks. The resulting nanosponges can be generated by simply mixing their components in aqueous buffer.

They are stable in size for up to 72 h. Therefore, in distinct contrast to classic liposomes, numerous applications can be envisioned in which the nanosponge will be long-term stored in desiccated form and mixed with aqueous buffer immediately before clinical use.

In recent years, cytotherapy has attracted massive attention as a targeting cancer therapy. Cytotherapy uses cancer targeting cells as delivery vehicles to carry therapeutics into the tumor site.[18,30,35,55–57,59,60] Studies have shown that macrophages are capable of delivering therapeutics to tumors sites.[55–57] We envision entrapping therapeutics into these nanovesicles, and then loading them into transport cells to achieve targeted delivery. However, the nanosponges themselves have to be non-toxic to ensure high survival rates during transport. Therefore, it is encouraging that virtually no toxic effects have been found during our initial cell proliferation tests with monocyte-macrophage-like cells.

Summary

Nanosponges form spontaneously by mixing two trimeric peptide building blocks, (cholesterol-$(K)_n$DEVDGC)$_3$-trimaleimide and (cholesterol-$(D)_n$DEVDGC)$_3$-trimaleimide (n = 5, 10, 15, 20) in aqueous buffers. The resulting sponge-like supramolecular aggregates are long-term stable and do not significantly change their diameter within 72 h. Their structure was elucidated with the help of Coarse-Grained Molecular Dynamics. Since the nanosponges were virtually non-toxic in cell experiments with monocyte/macrophage-like cells (RAW264.7 cells), they are promising candidates for drug-delivery to transporting cells in cytotherapy of solid tumors (leucocytes or stem cells). The fundamental features of this novel and structurally unique supramolecular system have been elucidated in this initial study. In further studies, we will investigate the suitability and adaptability of this system for tailored applications in targeted cancer therapy.

Appendix A. Supplementary data

Supplementary data to this article can be found online at http://dx.doi.org/10.1016/j.nano.2017.07.004.

References

1. Cassidy J, Schatzlein AG. Tumour-targeted drug and gene delivery: principles and concepts. *Expert Rev Mol Med* 2004;**6**(19):1-17.
2. Hamad I, Moghimi SM. Critical issues in site-specific targeting of solid tumours: the carrier, the tumour barriers and the bioavailable drug. *Expert Opin Drug Delivery* 2008;**5**(2):205-19.
3. Moses MA, Brem H, Langer R. Advancing the field of drug delivery: taking aim at cancer. *Cancer Cell* 2003;**4**(5):337-41.
4. Allen TM, Cullis PR. Drug delivery systems: entering the mainstream. *Science* 2004;**303**(5665):1818-22.
5. Tiwari G, Tiwari R, Sriwastawa B, Bhati L, Pandey S, Pandey P, et al. Drug delivery systems: an updated review. *Pharm Invest* 2012;**2**(1):1-11.
6. Devadasu VR, Bhardwaj V, Kumar MNVR. Can controversial nanotechnology promise drug delivery? *Chem Rev* 2013;**113**(3):1686-735.
7. Sawant RR, Torchilin VP. Liposomes as smart' pharmaceutical nanocarriers. *Soft Matter* 2010;**6**(17):4026-44.
8. Yapa AS, Bossmann SH. Development of magnetic theranostic agents. In: Bossmann SH, Wang H, editors. *Magnetic Nanomaterials: Applications in Catalysis and Life Sciences*. London: The Royal Society of Chemistry; 2017.
9. Yu M, Zheng J. Clearance pathways and tumor targeting of imaging nanoparticles. *ACS Nano* 2015;**9**(7):6655-74.
10. Nakamura Y, Mochida A, Choyke PL, Kobayashi H. Nanodrug delivery: is the enhanced permeability and retention effect sufficient for curing cancer? *Bioconjug Chem* 2016;**27**(10):2225-38.
11. Lytton-Jean AKR, Kauffman KJ, Kaczmarek JC, Langer R. Cancer nanotherapeutics in clinical trials. *Cancer Treat Res* 2015;**166**:293-322 [Nanotechnology-Based Precision Tools for the Detection and Treatment of Cancer].
12. Colletier J-P, Chaize B, Winterhalter M, Fournier D. Protein encapsulation in liposomes: efficiency depends on interactions between protein and phospholipid bilayer. *BMC Biotechnol* 2002;**2**:9.
13. Glavas-dodov M, Fredro-kumbaradzi E, Goracinova K, Calis S, Simonoska M, Hincal AA. 5-Fluorouracil in topical liposome gels for anticancer treatment - formulation and evaluation. *Acta Pharm* 2003;**53**(4):241-50.
14. Templeton NS, Lasic DD, Frederik PM, Strey HH, Roberts DD, Pavlakis GN. Improved DNA: liposome complexes for increased systemic delivery and gene expression. *Nat Biotechnol* 1997;**15**(7):647-52.
15. Yatvin MB, Weinstein JN, Dennis WH, Blumenthal R. Design of liposomes for enhanced local release of drugs by hyperthermia. *Science* 1978;**202**(4374):1290-3.
16. Mayer LD, Hope MJ, Cullis PR. Vesicles of variable sizes produced by a rapid extrusion procedure. *Biochim Biophys Acta* 1986;**858**(1):161-8.
17. Olson F, Hunt CA, Szoka FC, Vail WJ, Papahadjopoulos D. Preparation of liposomes of defined size distribution by extrusion through polycarbonate membranes. *Biochim Biophys Acta* 1979;**557**(1):9-23.
18. Basel MT, Shrestha TB, Troyer DL, Bossmann SH. Protease-sensitive, polymer-caged liposomes: a method for making highly targeted liposomes using triggered release. *ACS Nano* 2011;**5**(3):2162-75.
19. Gabizon AA, Shmeeda H, Zalipsky S. Pros and cons of the liposome platform in cancer drug targeting. *J Liposome Res* 2006;**16**(3):175-83.
20. van Hell AJ, Costa CICA, Flesch FM, Sutter M, Jiskoot W, Crommelin DJA, et al. Self-assembly of recombinant amphiphilic oligopeptides into vesicles. *Biomacromolecules* 2007;**8**(9):2753-61.
21. Holowka EP, Pochan DJ, Deming TJ. Charged polypeptide vesicles with controllable diameter. *J Am Chem Soc* 2005;**127**(35):12423-8.
22. Sukthankar P, Gudlur S, Avila LA, Whitaker SK, Katz BB, Hiromasa Y, et al. Branched oligopeptides form nanocapsules with lipid vesicle characteristics. *Langmuir* 2013;**29**(47):14648-54.
23. Sukthankar P, Whitaker SK, Garcia M, Herrera A, Boatwright M, Prakash O, et al. Thermally induced conformational transitions in nascent branched amphiphilic peptide capsules. *Langmuir* 2015;**31**(10):2946-55.
24. Avila LA, Aps LRMM, Sukthankar P, Ploscariu N, Gudlur S, Simo L, et al. Branched amphiphilic cationic oligopeptides form peptiplexes with DNA: a study of their biophysical properties and transfection efficiency. *Mol Pharm* 2015;**12**(3):706-15.
25. Jia Z, Whitaker SK, Tomich JM, Chen J. Organization and structure of branched amphipathic oligopeptide bilayers. *Langmuir* 2016;**32**(38):9883-91.
26. Danhier F. To exploit the tumor microenvironment: since the EPR effect fails in the clinic, what is the future of nanomedicine? *J Controll Release* 2016;**244**(Part_A):108-21.
27. Si J, Shao S, Shen Y, Wang K. Macrophages as active nanocarriers for targeted early and adjuvant cancer chemotherapy. *Small* 2016;**12**(37):5108-19.
28. Rachakatla RS, Balivada S, Seo G-M, Myers CB, Wang H, Samarakoon TN, et al. Attenuation of mouse melanoma by a/C magnetic field after delivery of bi-magnetic nanoparticles by neural progenitor cells. *ACS Nano* 2010;**4**(12):7093-104.
29. Heathman TRJ, Nienow AW, McCall MJ, Coopman K, Kara B, Hewitt CJ. The translation of cell-based therapies: clinical landscape and manufacturing challenges. *Regen Med* 2015;**10**(1):49-64.

30. Basel MT, Shrestha TB, Bossmann SH, Troyer DL. Cells as delivery vehicles for cancer therapeutics. *Ther Deliv* 2014;**5**(5):555-67.
31. Fontaine SD, Reid R, Robinson L, Ashley GW, Santi DV. Long-term stabilization of maleimide-thiol conjugates. *Bioconjug Chem* 2015;**26**(1):145-52.
32. Linder M, Tschernig T. Vasculogenic mimicry: possible role of effector caspase-3, caspase-6 and caspase-7. *Ann Anat* 2016;**204**:114-7.
33. Rich DH, Gesellchen PD, Tong A, Cheung A, Buckner CK. Alkylating derivatives of amino acids and peptides. Synthesis of N-maleoylamino acids, [1-(N-maleoylglycyl)cysteinyl]oxytocin, and [1-(N-maleoyl-11-aminoundecanoyl)cysteinyl]oxytocin. Effects on vasopressin-stimulated water loss from isolated toad bladder. *J Med Chem* 1975;**18**(10):1004-10.
34. Pieken, W.; Hill, K.; Eaton, B.; McGee, D.; Vagle, K.; Gold, L.; Stephens, A. Conjugating macromolecules using cycloaddition reactions. US6737236B1, 2004.
35. Wang H, Shrestha TB, Basel MT, Dani RK, Seo G-M, Balivada S, et al. Magnetic-Fe/Fe3O4-nanoparticle-bound SN38 as carboxylesterase-cleavable prodrug for the delivery to tumors within monocytes/macrophages. *Nanotechnol* 2012;**3**:444-55 [12 pp].
36. Coin I, Beyermann M, Bienert M. Solid-phase peptide synthesis: from standard procedures to the synthesis of difficult sequences. *Nat Protoc* 2007;**2**(12):3247-56.
37. Cheronis JC, Whalley ET, Nguyen KT, Eubanks SR, Allen LG, Duggan MJ, et al. A new class of bradykinin antagonists: synthesis and in vitro activity of bissuccinimidoalkane peptide dimers. *J Med Chem* 1992;**35**(9):1563-72.
38. Perera AS, Wang H, Basel MT, Pokhrel MR, Gamage PS, Kalita M, et al. Channel blocking of MspA revisited. *Langmuir* 2013;**29**(1):308-15.
39. https://mai.ku.edu/about-mai-lab.
40. Pronk S, Pall S, Schulz R, Larsson P, Bjelkmar P, Apostolov R, et al. GROMACS 4.5: a high-throughput and highly parallel open source molecular simulation toolkit. *Bioinformatics* 2013;**29**(7):845-54.
41. Bussi G, Donadio D, Parrinello M. Canonical sampling through velocity rescaling. *J Chem Phys* 2007;**126**(1):014101.
42. Berendsen HJC, Postma JPM, van Gunsteren WF, DiNola A, Haak JR. Molecular dynamics with coupling to an external bath. *J Chem Phys* 1984;**81**(8):3684-90.
43. Darden T, York D, Pedersen L. Particle mesh Ewald: an n.Log(N) method for Ewald sums in large systems. *J Chem Phys* 1993;**98**(12):10089-92.
44. Hess B, Bekker H, Berendsen HJC, Fraaije JGEM. LINCS: a linear constraint solver for molecular simulations. *J Comput Chem* 1997;**18**(12):1463-72.
45. Miyamoto S, Kollman PA. Settle: an analytical version of the SHAKE and RATTLE algorithm for rigid water models. *J Comput Chem* 1992;**13**(8):952-62.
46. Parrinello M, Rahman A. Polymorphic transitions in single crystals: a new molecular dynamics method. *J Appl Phys* 1981;**52**(12):7182-90.
47. Monticelli L, Kandasamy SK, Periole X, Larson RG, Tieleman DP, Marrink S-J. The MARTINI coarse-grained force field: extension to proteins. *J Chem Theory Comput* 2008;**4**(5):819-34.
48. Stockert JC, Blazquez-Castro A, Canete M, Horobin RW, Villanueva A. MTT assay for cell viability: intracellular localization of the formazan product is in lipid droplets. *Acta Histochem* 2012;**114**(8):785-96.
49. Bhattacharjee S. DLS and zeta potential — what they are and what they are not? *J Control Release* 2016;**235**:337-51.
50. https://imagej.nih.gov/nih-image/.
51. Chou PY, Scheraga HA. Calorimetric measurement of enthalpy change in the isothermal helix–coil transition of poly-L-lysine in aqueous solution. *Biopolymers* 1971;**10**(4):657-80.
52. Pivcova H, Saudek V. 13 C NMR relaxation study of poly (aspartic acid). *Polymer* 1985;**26**(5):667-72.
53. Saudek V, Stokrova S, Schmidt P. Conformational study of poly(alpha-L-aspartic acid). *Biopolymers* 1982;**21**(6):1011-20.
54. Ismail AA, Mantsch HH. Salt bridge induced changes in the secondary structure of ionic polypeptides. *Biopolymers* 1992;**32**(9):1181-6.
55. Basel MT, Balivada S, Shrestha TB, Seo G-M, Pyle MM, Tamura M, et al. A cell-delivered and cell-activated SN38-dextran prodrug increases survival in a murine disseminated pancreatic cancer model. *Small* 2012;**8**(6):913-20.
56. Seo G-M, Rachakatla RS, Balivada S, Pyle M, Shrestha TB, Basel MT, et al. A self-contained enzyme activating prodrug cytotherapy for preclinical melanoma. *Mol Biol Rep* 2012;**39**(1):157-65.
57. Basel MT, Balivada S, Wang H, Shrestha TB, Seo GM, Pyle M, et al. Cell-delivered magnetic nanoparticles caused hyperthermia-mediated increased survival in a murine pancreatic cancer model. *Nanomedicine* 2012;**7**:297-306.
58. Lehner R, Wang X, Marsch S, Hunziker P. Intelligent nanomaterials for medicine: carrier platforms and targeting strategies in the context of clinical application. *Nanomedicine* 2013;**9**(6):742-57.
59. Shrestha TB, Seo GM, Basel MT, Kalita M, Wang H, Villanueva D, et al. Stem cell-based photodynamic therapy. *Photochem Photobiol Sci* 2012;**11**(7):1251-8.
60. Alshetaiwi HS, Balivada S, Shrestha TB, Pyle M, Basel MT, Bossmann SH, et al. Luminol-based bioluminescence imaging of mouse mammary tumors. *J Photochem Photobiol B* 2013;**127**:223-8.